Check for updates

physica status solidi (a)

RESEARCH ARTICLE OPEN ACCESS

Setup for Long-Term Outdoor Testing of Optically Modified PV Modules Regarding their Thermal and Electrical Behavior Under Load

Moritz Ruhwedel[1,2] | Florian Sutter[1] | Stephan Heise[1] | Udayan Banik[1] | Peter Heller[1] | Robert Pitz-Paal[1,2]

[1]Institute of Solar Research, Deutsches Zentrum für Luft- und Raumfahrt e. V., Köln, Germany | [2]Chair of Solar Technology, RWTH Aachen University, Köln, Germany

Correspondence: Moritz Ruhwedel (Moritz.Ruhwedel@dlr.de)

Received: 5 November 2025 | **Accepted:** 12 November 2025

Keywords: anti-reflective | anti-soiling | passive radiative cooling | photovoltaic | PV-mirror

ABSTRACT

Optical modifications of the light-facing side of photovoltaic (PV) modules can be used to increase their efficiency by implementing anti-reflective or anti-soiling properties or by achieving a reduction of the operating temperature. Furthermore, such front-optical modifications can be utilized to hybridize concentrating solar thermal systems and PV systems. In order to characterize such modifications correctly, special attention has to be paid to two points: the modules have to be operated under load to keep the cells at a realistic operating temperature, and high precision of the temperature measurement is required to quantify the potentially very small effects of the modifications (e.g., for radiative cooling decreases in operating temperature of less than 1 K have to be expected). In this paper, a setup is presented for testing front-optical modifications in fixed tilt configuration in Almería, Spain. The loading is achieved by the use of an electronic load and the precision of the temperature measurement is achieved by Platinum resistance temperature detectors (Pt100s) laminated into the modules in combination with high precision multimeters. To demonstrate the capabilities of the setup, exemplary measurement data is shown.

1 | Introduction

Modifications of the light-facing side of PV modules are commonly used to increase the efficiency of the PV modules. For instance, over 90% of commercial PV modules are nowadays supplied with anti-reflective coatings [1]. The various benefits of front-optical modifications for the PV module operation can be categorized into three groups: anti-reflective properties, anti-soiling properties, and the reduction of operating temperature. In the following it is summarized which effects common front-optical modifications have on the electrical and thermal behavior of PV modules and what the resulting requirements for a measurement setup to characterize them are.

Anti-reflective modifications increase PV module efficiency by reducing the fraction of incident power being reflected at the front surface of the module. Under normal incidence about 4% of the incident power is lost at an air–glass surface. Ideally only the transmission above the bandgap is increased as increased sub-bandgap transmission only leads to increased operating temperatures. Usually, anti-reflective modifications are realized by single layer porous SiO_2 coatings leading to about 2%–3% increase of output power under standard testing conditions [2, 3]. Another option to achieve anti-reflective properties is to use multilayer coatings made of alternating layers of low and high refractive index. They offer increased durability [4] and potentially better performance depending on the number of layers [1]. The production of multilayer coatings, however, is more expensive so that they are currently less common than porous SiO_2 monolayers. Anti-reflective properties can also be achieved by using textured glass as front cover [5–7]. As example, the commercial Saint Gobain Alberino product line was shown to increase the short circuit current of modules

This is an open access article under the terms of the Creative Commons Attribution License, which permits use, distribution and reproduction in any medium, provided the original work is properly cited.

© 2025 The Author(s). *physica status solidi (a)* applications and materials science published by Wiley-VCH GmbH.

utilizing it by up to 3.2% in a solar simulator under normal incidence [8].

Soiling on the module surface can significantly reduce the light transmitted to the underlying PV cells and thus its efficiency [9, 10]. Ilse et al. assumed the loss in global solar energy production (PV and concentrating solar power) to be at least 3%–4% in 2018 [11]. Regular cleaning is required to maintain optimal performance depending on the soiling conditions. Additionally, anti-soiling coatings for preventing soiling and simplifying the cleaning are being developed. Anti-soiling properties of the module surface are achieved by equipping it with either hydrophobic or hydrophilic properties. Furthermore, photocatalytic properties can be utilized to decompose organic compounds and thus enhance the self-cleaning or simplify the manual cleaning [12]. A variety of different approaches exist to achieve anti-soiling coatings [13]. Anti-soiling properties also can be accomplished using surface texturing [14, 15]. Ideally, anti-soiling coatings are designed in a way that they also exhibit anti-reflective properties. Covestro (Covestro Deutschland AG, Kaiser-Wilhelm-Allee 60, 51373 Leverkusen, Germany), for example, claims an average transmission gain of ≈3% of their anti-soiling coating compared to uncoated glass [16].

A reduction of the operating temperature can be achieved with front-optical modifications by either reflecting sub-bandgap (or UV) irradiation to avoid parasitic absorption [17, 18] or by increasing the IR emissivity of the front surface to facilitate passive radiative cooling (PRC) [18–22]. Monocrystalline silicon PV loses about 0.45% of its efficiency per 1 K increase of its operating temperature [23] meaning that for an operating temperature of 50°C the efficiency is reduced by over 10% compared to standard testing conditions. With a bandgap of 1.1 eV, the sub-bandgap radiation, which is partially absorbed in the module stack and thus transformed into heat, makes up about 20% of the incident power of the AM1.5 spectrum. Under steady-state conditions an ideal sub-bandgap reflector was simulated to reduce the operating temperature of a PV module up to about 5 K compared to a module without anti-reflective coating [24]. A simulation of 1 year of operation of a module utilizing an ideal sub-bandgap reflector in Golden, Colorado, USA yielded an irradiance-weighted mean average temperature decrease of 3.8 K compared to a module without anti-reflective coating [25].

PRC refers to passively cooling an object by utilizing radiative heat transfer to potential heat sinks, most importantly: space [26–28]. This requires a high emissivity of the object especially in the wavelength range where the atmosphere is transparent, the atmospheric window. If the object to be cooled has a lower temperature than the atmosphere the emissivity should be low for other wavelengths to avoid absorbing heat from it. As PV modules, however, operate at higher temperature than the ambient air for them high-emissivity over the whole wavelength range is beneficial. A simulation of 1 year of operation of a module with an emissivity of 1 at the front surface in Golden, Colorado, USA predicted an irradiance-weighted mean average temperature decrease of 0.8 K compared to a reference module without any front-optical modifications [25].

A second purpose of front-optical modifications can be the use of PV modules as PV-Mirrors to hybridize photovoltaic and concentrating solar thermal (CST) systems [29–34]. In this concept the solar mirrors in a CST system are replaced by PV modules with spectrally selective coatings to partially transmit the incident spectrum to the PV cells and reflect the rest to the CST receiver. On the PV side this is similar to the aforementioned use of spectrally selective reflectors to reduce the operating temperature of PV cells. The quantitative advantages of this concept are yet to be proven and are largely dependent on the way the spectrum is split and the used CST configuration [34].

In this article, a setup is presented for testing all types of front-optical modifications. Particular attention is paid to two points: First, the modules must be operated under load with adequate tracking of their maximum power point (MPP) to achieve realistic operating temperatures. Second, precise measurement of the electrical parameters and the cell temperature are required to be able to resolve the often small effects of the front-optical modifications on the electrical and thermal performance of the modules. While precise electrical measurements can be easily achieved by choosing appropriate measurement equipment more attention has to paid when trying to measure the cell temperature.

One way to determine the cell temperature is deriving it from the open-circuit voltage according to IEC 60904–5 [35]. Although very precise if applicable, this method has some drawbacks that might make direct measurement of the cell temperature unavoidable in some cases. In IEC 60904–5, it is stated that the method should be only applied for irradiances above 400 Wm^{-2}. For front-optical modifications that reduce the transmitted irradiance to the cell (as can be the case for, e.g., the PV-Mirror) the minimum required irradiance is increased. Further, IEC 60904–5 is not applicable anymore if the irradiance that is transmitted to the cell is strongly dependent on the angle of incidence, as it might be the case for multilayer stacks. In this case knowledge of the angular behavior of the transmission to the cell and appropriate adaption of IEC 60904–5 would be required. Moreover, it was found that unprecise knowledge of the PV cells' diode ideality factor and variations of it with irradiance and temperature can introduce significant errors in the determined cell temperature [36, 37].

When directly measuring the cell temperature, it is important where to place the temperature sensors. Jankovec and Topič compared different ways to measure the cell temperature of PV modules [38]. They could only achieve an average deviation of measured and actual cell temperature of under 1 K by using Platinum resistance temperature detectors (Pt1000s) laminated into the module as close as possible to the cell. However, test setups often lack accuracy of the temperature measurement because the cell temperature is only measured on the outside of the module and/or only with thermocouples which have a limited precision [25, 39, 40]. Jankovec and Topič showed that for temperature measurements on the outside of the module, covers should be used as otherwise the measurements can be strongly affected by environmental conditions [38]. In the aforementioned setups no covering of the temperature sensors is mentioned [25, 39, 40]. Furthermore, if the temperature of the module is measured on the outside of the module, only the surface temperature of the module is obtained, which might deviate from the cell temperature by several Kelvin [38].

In this publication, a setup is presented for long-term outdoor testing of front-optical modifications of PV modules. Based on the state-of-the-art, a single-cell reference module design was

18626319, 0, Downloaded from https://onlinelibrary.wiley.com/doi/10.1002/pssa.202500919 by Dtsch Zentrum F. Luft-U. Raum Fahrt In D. Helmholtz Gemein., Wiley Online Library on [27/11/2025]. See the Terms and Conditions (https://onlinelibrary.wiley.com/terms-and-conditions) on Wiley Online Library for rules of use; OA articles are governed by the applicable Creative Commons License

developed for testing of the front-optical modifications to ensure comparability of the results. Front-optical modifications can be applied to its $25 \times 25\,cm^2$ cover glass. The modified modules alongside an unmodified reference module can be mounted in fixed-tilt configuration at the Plataforma Solar de Almería (PSA), owned by the Centro de Investigaciones Energéticas, Medioambientales y Tecnológicas (CIEMAT), in southern Spain and tested under arid climate. The operation under load and the MPP tracking are achieved by an electronic load. Additionally to the option to derive the cell temperature from the open-circuit voltage it is directly measured using 4 Platinum resistance temperature detectors (Pt100s) laminated as close as possible to each cell. Measurement of the cell temperature at different points is required as the temperature distribution of only a single cell, that is not part of a module, might be very inhomogeneous. The effect of different front-optical modifications on the cell temperature may vary between its application in a full-scale module and the single-cell modules used here. However, the use of small single-cell modules allows for the testing of modifications developed at lab scale.

1 day of measurement of a module without any front-optical modifications is presented and the average operating temperature over a period of 3 months of a module with and without connection to the load is compared.

2 | Methods

2.1 | Reference Module Design

According to the 16th edition of the International Technology Roadmap for Photovoltaics the predominant PV cell technology in 2024 was TOPCon [41]. About 90% of the cells in the market were bifacial, the predominant wafer size was M10, almost all modules were employing half-cells and more than half of all cells in the market were using more than 12 busbars or busbarless technology. A shift toward larger cell dimensions and an increasing share of busbarless cells in the next years is predicted. Therefore, bifacial TOPCon half-cells were used for the reference module design. For reasons of availability and manageability M6 wafers with 9 busbars were used. The cells were manufactured and characterized by ISC Konstanz e.V. (International Solar Energy Research Center Konstanz, ISC Konstanz e.V., Rudolf-Diesel-Straße 15, 78467 Konstanz, Germany). Their average characteristics at standard testing conditions (STC) can be found in Table 1.

TABLE 1 | Average characteristics of used TOPCon half-cells under STC.

Efficiency %	V_{OC} V	I_{SC} A	V_{MPP} V	I_{MPP} A	P_{MPP} W	FF %
22.7	0.702	5.476	0.603	5.168	3.16	81.05

1 and 3 mm float glass (AGC SunMax Premium) was used as front-cover and back-cover, respectively, to provide mechanical stability. Polyolefin (POE, Mitsui Chemicals Solar Asce: TR01BA-45T) was used as encapsulant, since EVA/POE mixtures and POE are expected to dominate the market in the future even though ethylene vinyl acetate (EVA) still has the biggest market share due to its cost efficiency [41]. Furthermore, POE exhibits better degradation-resistive behavior in glass–glass modules than EVA [42, 43]. The used POE is supplied in foils of 0.63 mm thickness. The schematic structure of the modules is shown in Figure 1.

On the front of the PV cells, one layer of POE foil was used as in a commercial PV module. On the back, 4 layers were used to accommodate the 1.0 mm thick Pt100s without breaking the cells: one layer of POE was put in between the PV cells and the Pt100s, and 3 layers were put between the Pt100s and the rear glass. The Pt100 sensors (Yageo Nexensos Pt100 L220 F 0.1 (1/3 B)) are of tolerance class F 0.1 (1/3B) meaning the measurement error is given by $\pm(0.1°C + 0.0017 \cdot T)$ for temperatures between 0 and 150°C with T denoting the temperature in °C [44, 45]. In Figure 1a the marked outer (I) and inner (II) surface of the front glass indicate the possible surfaces for the implementation of front-optical modifications.

The cells were hand-soldered using PV ribbon (Ulbrich of Austria GmbH Standard PV Ribbon) and the Pt100s were contacted using enameled copper wire of 0.5 mm diameter in a 4-wire configuration. The layout of the Pt100s is shown in the rear-view of the modules in Figure 1b. They are placed in the top left corner (B_1),

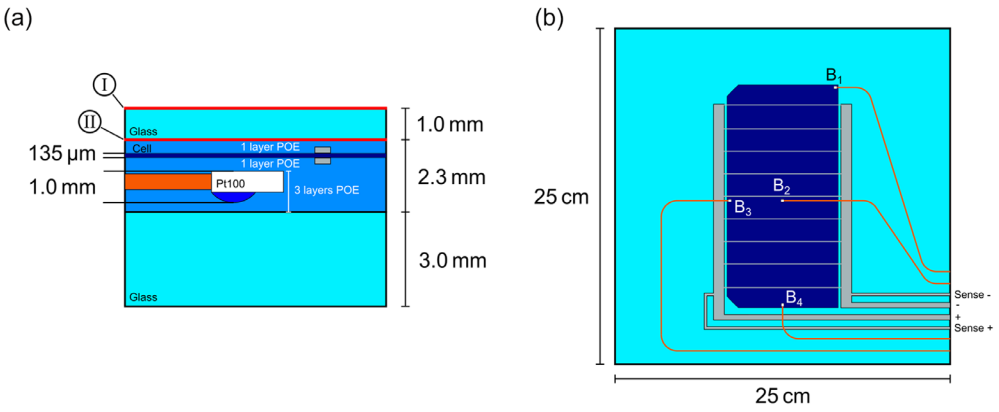

FIGURE 1 | Schematic design of the reference PV module design used to compare different front-optical modifications. (a) Cross-sectional view of the module with the possible surfaces for the application of front-optical modifications denoted by I and II. (b) Rear-view showing the positions of the PV cell and the Pt100 sensors B_1 to B_4. Sense + and Sense - are for voltage probing as close to the cell as possible. Further details can be found in the Supporting Information.

18625319, 0, Downloaded from https://onlinelibrary.wiley.com/doi/10.1002/pssa.202500919 by Dtsch Zentrum F. Luft-U. Raum Fahrt In D. Helmholtz Gemein., Wiley Online Library on [27/11/2025]. See the Terms and Conditions (https://onlinelibrary.wiley.com/terms-and-conditions) on Wiley Online Library for rules of use; OA articles are governed by the applicable Creative Commons License

the center (B_2), the middle of the right edge (B_3), and the middle of the bottom edge (B_4) to be able to measure the temperature distribution of the cell. The tolerance of the positioning due to the movement of the encapsulant during lamination is estimated to be ±4 mm in the module plane, being lower for B_2 in the middle of the module. The wires for voltage sensing of the solar cell are connected as close as possible to the cell to avoid voltage drops. All wires are routed out of the module at the bottom right corner. The assembled modules were laminated in a membrane laminator (P. Energy Laminator 094A, for details see the Supporting Information).

2.2 | Measurement Setup

The test rack (as shown in Figure 2), which can accommodate 6 modules, was installed at the testing location in southern Spain (PSA). This location was chosen as it provides high solar resource.

The modules are mounted in the module frame in fixed-tilt configuration at a height of 1.5 m to reduce the influence of the shadows cast by them on the irradiation from the backside. They are mounted facing south and the tilt-angle of 35° was optimized using PVGIS [46] for maximum yield. Two pyranometers (Kipp und Zonen CMP 10) are mounted in the same plane as the modules (Figure 2a), one facing to the front, one facing to the back to measure the in-plane irradiance on the front and the back of the modules. Weather data is available from a meteorological station nearby. Shielded cables were soldered directly to the modules, and the soldering joints were placed in a protected junction box (Figure 2c–e) casted with silicone gel. The measurement electronics are located inside a climatized container nearby.

The temperature and irradiance measurements are carried out using two digital multimeters (DMMs, Agilent 34972A) utilizing several multiplexer cards (Agilent 34901A, Agilent 34902A). The DMMs allow for an accuracy of 0.06 K of the temperature measurement [47].

Only two modules at a time can be connected to the load for the electrical measurements as it only has two channels. In the current configuration, each day, a different module is measured alongside with the reference module. The schematic for the measurement electronics for the electrical measurement of the modules is shown in Figure 3.

A variable electronic load (Keysight EL34243A) in series with a DC source (Keysight E36233A) is used to allow for the simultaneous operation under load and the measurements of the IV curves. Electronic loads usually require a voltage of over 3 V across their terminals to be able to properly regulate voltage or current [48]. Furthermore, at high currents more than 1 V drops at the wiring to the modules. As IV curves should be measured down to nearly 0 V at the cells, where the modules produce the highest currents, the DC source in series with the modules is required to provide these voltages. The voltage across the modules is measured at the sense outputs of the modules. The reference module is connected at all times to channel 1 of load and DC source, while a multiplexer is used to switch between the modules of interest on channel 2 of load and DC source.

A visualization of the measurement routine during daytime can be found in Figure 4.

A complete IV curve is measured every 3 min together with the temperatures of the cells and the front and backside irradiance. MPP tracking is done by measuring and evaluating the IV curve between 0.5 and 0.73 V every 20 s. The daytime measurement routine starts 30 min before sunrise and ends 30 min after sunset.

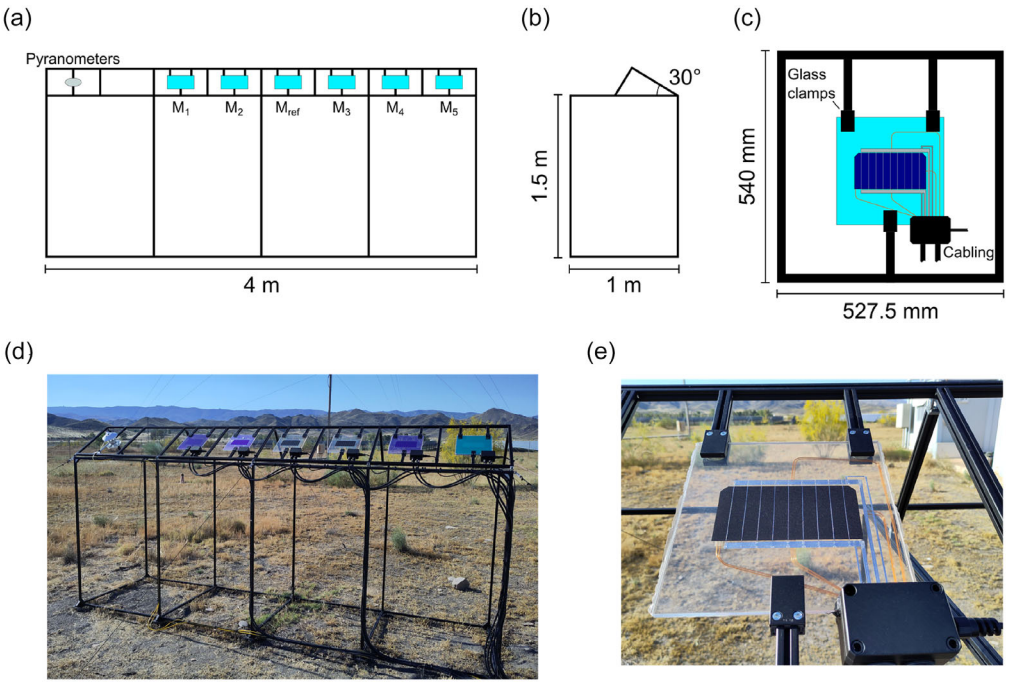

FIGURE 2 | Racking for the modules under test. Drawing of (a) the front and (b) the side of the rack. (c) Drawing one of the individual segments of the module frame. (d) Photography of the actual rack with 6 modules to be tested. (e) Photography of one installed module. The test rack is installed at the PSA, owned by CIEMAT.

18626319, 0, Downloaded from https://onlinelibrary.wiley.com/doi/10.1002/pssa.202500919 by Dtsch Zentrum F. Luft-U. Raum Fahrt In D. Helmholtz Gemein., Wiley Online Library on [27/11/2025]. See the Terms and Conditions (https://onlinelibrary.wiley.com/terms-and-conditions) on Wiley Online Library for rules of use; OA articles are governed by the applicable Creative Commons License

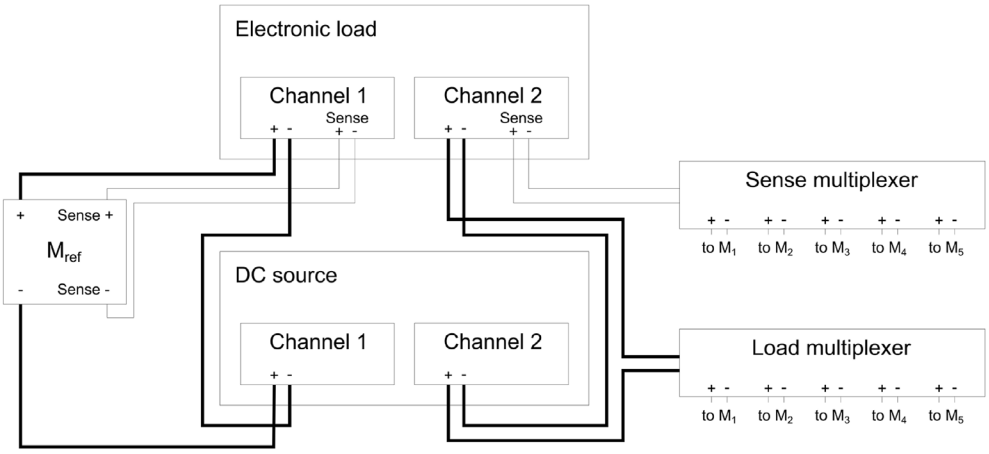

FIGURE 3 | Schematic of the system for the electrical measurement of the reference module (M_{ref}) and the test modules M_1 to M_5.

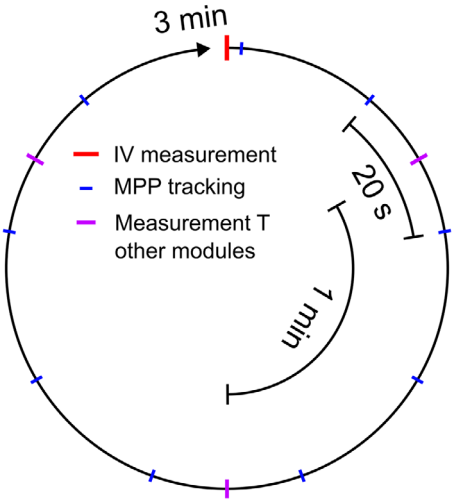

FIGURE 4 | One measurement cycle during daytime. Modules are operated in MPP permanently except during IV curve measurements and MPP tracking.

During night time all modules are disconnected from the load and the DC source. The temperature of the modules that are currently not under load together with the front and backside irradiance is measured once a minute during day time. The temperature of the modules connected to the load is only measured when an IV curve is measured. During night time the temperature of all modules is measured every minute.

3 | Results

To illustrate the performance of the measurement system, a 1-day measurement of the reference module (without any front-optical modification) is shown in Figure 5 (June 13, 2025) including irradiance, the temperatures of B_1–B_4, T_1–T_4 respectively, the output power in MPP and V_{OC} and I_{SC}.

In the morning during times with very low irradiance, it can be seen that T_1–T_4 are identical within the error boundaries of the temperature measurement. This is a confirmation of the precision of the temperature measurement of the different Pt100s as during night without illumination the modules should be homogeneous in temperature. Furthermore, it can be seen that the module temperature during this time is about 2 K lower than the air temperature. This is because of the high emissivity of glass

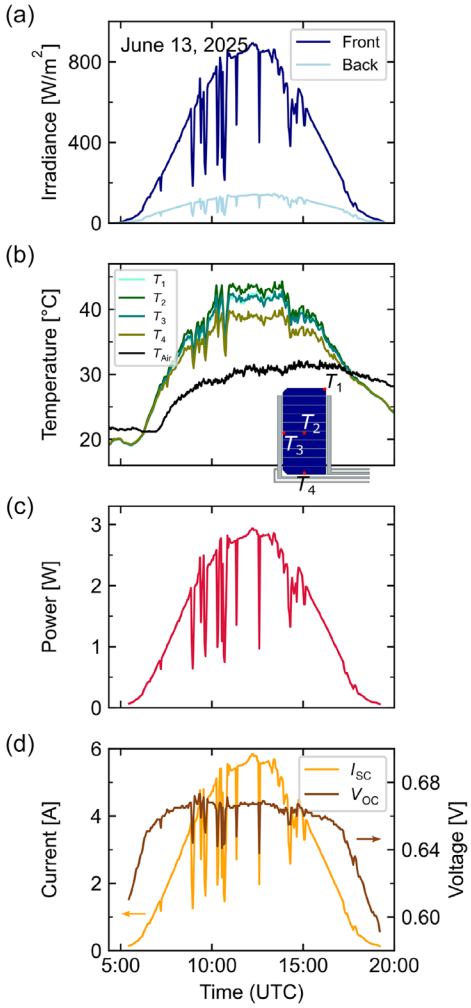

FIGURE 5 | Exemplary results of 1 day (June 13, 2025) of measurement of a PV module without any front-optical modifications: (a) irradiance on front and back, (b) temperatures of B_1–B_4, T_1–T_4, respectively, and the ambient air temperature T_{Air} (including a back view of the cell with the positions of the temperature measurements), (c) output power, and (d) I_{SC} and V_{OC} of the module.

18626319, 0, Downloaded from https://onlinelibrary.wiley.com/doi/10.1002/pssa.202500919 by Dtsch Zentrum F. Luft-U. Raum Fahrt In D. Helmholtz Gemein., Wiley Online Library on [27/11/2025]. See the Terms and Conditions (https://onlinelibrary.wiley.com/terms-and-conditions) on Wiley Online Library for rules of use; OA articles are governed by the applicable Creative Commons License

and the resulting PRC. During daytime, T_2 in the middle of the module is the highest, while T_4 is the lowest. T_1 and T_3 are very similar. This seems counterintuitive as B_1 in the corner would be expected to show a lower temperature than B_3 and B_4, which have a larger part of the PV cell in their proximity. Altogether, this might hint toward an asymmetric temperature distribution of the cell and/or a different distance of the Pt100s to the rear surface of the cell. An inhomogeneous temperature distribution could be explained by the copper ribbon close to three edges of the cells. It has a high thermal conductivity and thus can transport heat away from the cell while being highly reflective and thus it is not heated up a lot by the incident radiation. T_1–T_4 vary up to around 4°C throughout the day, which shows how important it is to not only measure the cell temperature in the middle of the cell.

As stated above the uncertainty of the placement of the Pt100 is 4 mm. It is assumed that the temperature gradient derived from the difference of T_2 to T_1, T_3, and T_4 is an upper bound for the temperature gradient at the positions of the respective Pt100 in any direction. From the average temperature gradients calculated this way in the time from May 29, 2025 to September 7, 2025 for the reference module with connection to the load the error in temperature measurement due to displacement of the Pt100 is assumed to be 0.08 K.

To show the effect of the load on the operating temperature of the modules the average temperature of B_2, T_2, for one module under test was evaluated in the time from May 29, 2025 to September 7, 2025 for times with and without connection to the load during daytime. This could not be done for the reference module as the reference module is connected to the load all the time. The electrical output of this test module was slightly higher (≈2%) than that of the reference module. During times with connection to the load the average of T_2 was 36.6°C. During times without connection to the load the average of T_2 was 38.8°C leading to a difference of the average T_2 with and without load of −2.2°C. The actual temperature reduction at a certain state of operation is highly dependent on a lot of parameters, e.g. irradiance, air temperature, and wind speed, and might strongly differ from this value.

4 | Conclusion

In this work, a setup for long-term outdoor testing of the effects of front-optical modifications of PV modules on their operating temperature and their electrical output is presented. Special attention is paid to two points: operation under load and MPP tracking to ensure realistic operation conditions and precision of electrical and temperature measurement. Operation under load, MPP tracking and precision of the electrical measurements is achieved by the use of an electronic load. This feature has shown to reduce the cell temperature by more than 2 K compared to modules not connected to an electronic load. Precision of the temperature measurement is enabled by the use of precise Platinum resistance temperature detectors laminated as close as possible to the PV cells in combination with precise multimeters.

High precision of the measurements is required as different front-optical modifications may only have small effects on the electrical and thermal behavior of PV modules. 1 day of measurement of a module without any optical modification is shown to demonstrate the functionality of the setup. The effect of the usage of a load on the operating temperature is evaluated by comparing the average operating temperature over a period of 3 months of one module with and without connection to the load.

In the future, it is planned to use this setup to investigate different spectrally selective coatings (PV-Mirrors) as well as radiative cooling coatings.

Acknowledgments

The authors would like to sincerely thank Claas Koch, David Muruve Tejada, Christoph Ruhwedel, and Sergio Gonzalez Rodriguez who supported the creation of the experimental setup described in this publication with great technological knowledge. Without their help the setup could not have been developed. Furthermore, the work was supported by the Spanish research institution CIEMAT that owns the PSA at which the test site is located. Open Access funding enabled and organized by Projekt DEAL.

Conflicts of Interest

The authors declare no conflicts of interest.

Data Availability Statement

The data that support the findings of this study are available from the corresponding author upon reasonable request.

References

1. A. M. Law, L. O. Jones, and J. M. Walls, "The Performance and Durability of Anti-Reflection Coatings for Solar Module Cover Glass – A Review," *Solar Energy* 261 (2023): 85–95, https://doi.org/10.1016/j.solener.2023.06.009.

2. J. Wohlgemuth, D. Cunningham, J. Shaner, A. Nguyen, S. Ransome, and A. Artigao, in *Conference Record of the Thirty-first IEEE Photovoltaic Specialists Conference* (IEEE, 2005), 1015–1018.

3. C. Ballif, J. Dicker, D. Borchert, and T. Hofmann, "Solar Glass with Industrial Porous SiO2 Antireflection Coating: Measurements of Photovoltaic Module Properties Improvement and Modelling of Yearly Energy Yield Gain," *Solar Energy Materials and Solar Cells* 82 (2004): 331–344, https://doi.org/10.1016/j.solmat.2003.12.004.

4. J. M. Newkirk, I. Nayshevsky, A. Sinha, et al., "Artificial Linear Brush Abrasion of Coatings for Photovoltaic Module First-Surfaces," *Solar Energy Materials and Solar Cells* 219 (2021): 110757, https://doi.org/10.1016/j.solmat.2020.110757.

5. U. Blieske, T. Doege, P. Gayout, M. Neander, D. Neumann, and A. Prat, in *Proceedings of 3rd World Conference on Photovoltaic Energy Conversion* (IEEE, 2003).

6. D.-W. Kang, H.-M. Lee, and M.-K. Han, "Efficient Light Incoupling into Silicon Thin-Film Solar Cells by Anti-Reflecting Mgo/High-Compact-AZO with Air-Side Textured Glass," *Journal of Physics D: Applied Physics* 46 (2013): 485107, https://doi.org/10.1088/0022-3727/46/48/485107.

7. C. L. Pinto, I. Cornago, A. Buceta, E. Zugasti, and J. Bengoechea, "Random Subwavelength Structures on Glass to Improve Photovoltaic Module Performance," *Solar Energy Materials and Solar Cells* 246 (2022): 111935, https://doi.org/10.1016/j.solmat.2022.111935.

8. J. Jaus, M. Duell, J. Eckert, et al., in *SPIE Proceedings*, ed. N. G. Dhere, J. H. Wohlgemuth, K. Lynn (SPIE, 2010), 7773, https://doi.org/10.1117/12.863081.

18626319, 0, Downloaded from https://onlinelibrary.wiley.com/doi/10.1002/pssa.202500919 by Dtsch Zentrum F. Luft-U. Raum Fahrt In D. Helmholtz Gemein., Wiley Online Library on [27/11/2025]. See the Terms and Conditions (https://onlinelibrary.wiley.com/terms-and-conditions) on Wiley Online Library for rules of use; OA articles are governed by the applicable Creative Commons License

9. M. R. Maghami, H. Hizam, C. Gomes, M. A. Radzi, M. I. Rezadad, and S. Hajighorbani, "Power Loss Due to Soiling on Solar Panel: A Review," *Renewable and Sustainable Energy Reviews* 59 (2016): 1307–1316, https://doi.org/10.1016/j.rser.2016.01.044.

10. T. Sarver, A. Al-Qaraghuli, and L. L. Kazmerski, "A Comprehensive Review of the Impact of Dust on the Use of Solar Energy: History, Investigations, Results, Literature, and Mitigation Approaches," *Renewable and Sustainable Energy Reviews* 22 (2013): 698–733, https://doi.org/10.1016/j.rser.2012.12.065.

11. K. Ilse, L. Micheli, B. W. Figgis, et al., "Techno-Economic Assessment of Soiling Losses and Mitigation Strategies for Solar Power Generation," *Joule* 3 (2019): 2303–2321, https://doi.org/10.1016/j.joule.2019.08.019.

12. I. Arabatzis, N. Todorova, I. Fasaki, et al., "Photocatalytic, Self-Cleaning, Antireflective Coating for Photovoltaic Panels: Characterization and Monitoring in Real Conditions," *Solar Energy* 159 (2018): 251–259, https://doi.org/10.1016/j.solener.2017.10.088.

13. N. Sakarapunthip, M. Nukunudompanich, O. Sittipunsakda, et al., "Comparative Analysis of Anti-Soiling Coatings for PV Modules in a Tropical Climate," *Materials Chemistry and Physics* 345 (2025): 131284, https://doi.org/10.1016/j.matchemphys.2025.131284.

14. P. Tobosque, J. Núñez, A. Elgueda, L. Morán, and C. Carrasco, "Modifying the Surface Roughness of Solar Glass: A Passive Mitigation Method of Soiling," *Sustainable Energy Technologies and Assessments* 81 (2025): 104447, https://doi.org/10.1016/j.seta.2025.104447.

15. A. Roslizar, S. Dottermusch, R. Schmager, et al., "Hot-Embossed Microcone-Textured Fluoropolymer as Self-Cleaning and Anti-Reflective Photovoltaic Module Covers," *Solar Energy Materials and Solar Cells* 214 (2020): 110582, https://doi.org/10.1016/j.solmat.2020.110582.

16. "*Covestro Anti-Soiling Coating for Solar Glass*," Accessed September 9, 2025, https://solutions.covestro.com/-/media/covestro/solution-center/brochures/pdf/solar_anti_soiling_coating_v19002_factsheet_en_digital.pdf?rev=37b217a7ebb447cb898f389b903c0d39.

17. I. M. Slauch, M. G. Deceglie, T. J. Silverman, and V. E. Ferry, "Model for Characterization and Optimization of Spectrally Selective Structures to Reduce the Operating Temperature and Improve the Energy Yield of Photovoltaic Modules," *ACS Applied Energy Materials* 2 (2019): 3614–3623, https://doi.org/10.1021/acsaem.9b00347.

18. H. Meddeb, M. Götz-Köhler, N. Neugebohrn, et al., "Tunable Photovoltaics: Adapting Solar Cell Technologies to Versatile Applications," *Advanced Energy Materials* 12 (2022): 2200713, https://doi.org/10.1002/aenm.202200713.

19. D. Sato and N. Yamada, "Review of Photovoltaic Module Cooling Methods and Performance Evaluation of the Radiative Cooling Method," *Renewable and Sustainable Energy Reviews* 104 (2019): 151–166, https://doi.org/10.1016/j.rser.2018.12.051.

20. L. Zhu, A. Raman, K. X. Wang, M. A. Anoma, and S. Fan, "Radiative cooling of solar cells," *Optica* 1 (2014): 32, https://doi.org/10.1364/OPTICA.1.000032.

21. L. Zhu, A. P. Raman, and S. Fan, "Radiative Cooling of Solar Absorbers Using a Visibly Transparent Photonic Crystal Thermal Blackbody," *Proceedings of the National Academy of Sciences of the United States of America* 112 (2015): 12282–12287, https://doi.org/10.1073/pnas.1509453112.

22. U. Banik, K. Sasaki, N. Reininghaus, et al., "Enhancing Passive Radiative Cooling Properties of Flexible CIGS Solar Cells for Space Applications using Single Layer Silicon Oxycarbonitride Films," *Solar Energy Materials and Solar Cells* 209 (2020): 110456, https://doi.org/10.1016/j.solmat.2020.110456.

23. S. Ponce-Alcántara, J. P. Connolly, G. Sánchez, J. M. Míguez, V. Hoffmann, and R. Ordás, "A Statistical Analysis of the Temperature Coefficients of Industrial Silicon Solar Cells," *Energy Procedia* 55 (2014): 578–588, https://doi.org/10.1016/j.egypro.2014.08.029.

24. X. Sun, T. J. Silverman, Z. Zhou, M. R. Khan, P. Bermel, and M. A. Alam, "Optics-Based Approach to Thermal Management of Photovoltaics: Selective-Spectral and Radiative Cooling," *IEEE Journal of Photovoltaics* 7 (2017): 566–574, https://doi.org/10.1109/JPHOTOV.2016.2646062.

25. T. J. Silverman, M. G. Deceglie, I. Subedi, et al., "Reducing Operating Temperature in Photovoltaic Modules," *IEEE Journal of Photovoltaics* 8 (2018): 532–540, https://doi.org/10.1109/JPHOTOV.2017.2779842.

26. M. M. Hossain and M. Gu, "Radiative Cooling: Principles, Progress, and Potentials," *Advanced Science* 3 (2016): 1500360, https://doi.org/10.1002/advs.201500360.

27. U. Banik, A. Agrawal, H. Meddeb, et al., "Efficient Thin Polymer Coating as a Selective Thermal Emitter for Passive Daytime Radiative Cooling," *ACS Applied Materials & Interfaces* 13 (2021): 24130–24137, https://doi.org/10.1021/acsami.1c04056.

28. U. Banik, H. Meddeb, D. Berends, et al., "Impact of Parasitic Heat Fluxes on Deep Sub-ambient Radiative Coolers Under Variable Pressure," *Applied Thermal Engineering* 237 (2024): 121655, https://doi.org/10.1016/j.applthermaleng.2023.121655.

29. Z. J. Yu, K. C. Fisher, B. M. Wheelwright, R. P. Angel, and Z. C. Holman, "PVMirror: A New Concept for Tandem Solar Cells and Hybrid Solar Converters," *IEEE Journal of Photovoltaics* 5 (2015): 1791–1799, https://doi.org/10.1109/JPHOTOV.2015.2458571.

30. Z. J. Yu, K. C. Fisher, and Z. C. Holman, in *IEEE 42nd Photovoltaic Specialist Conference (PVSC)* (IEEE, 2015), 1–4.

31. K. Fisher, Z. Yu, R. Striling, and Z. Holman, in *AIP Conference Proceedings* (AIP, 2017), 20004.

32. Z. J. Yu, K. C. Fisher, X. Meng, J. J. Hyatt, R. P. Angel, and Z. C. Holman, "GaAs/Silicon PVMirror Tandem Photovoltaic Mini-module with 29.6% Efficiency with Respect to the Outdoor Global Irradiance," *Progress in Photovoltaics: Research and Applications* 27 (2019): 469–475, https://doi.org/10.1002/pip.3095.

33. D. Ziyati, A. Dollet, G. Flamant, Y. Volut, E. Guillot, and A. Vossier, "A Multiphysics Model of Large-Scale Compact PV–CSP Hybrid Plants," *Applied Energy* 288 (2021): 116644, https://doi.org/10.1016/j.apenergy.2021.116644.

34. M. Ruhwedel, K. Gehrke, E. Lüpfert, F. Sutter, P. Heller, and R. Pitz-Paal, "Integrated Concentrating Solar/Photovoltaic Hybrid Concepts—Technological Discussion, Energy Yield, and Cost Considerations," *Energy Technology* 12 (2024), https://doi.org/10.1002/ente.202301181.

35. IEC 60904-5:2011+AMD1:2022 CSV (Consolidated Version), Photovoltaic devices - Part 5: Determination of the equivalent cell temperature (ECT) of photovoltaic (PV) devices by the open-circuit voltage method, 27.160 (IEC, 2022).

36. G. H. Yordanov, O.-M. Midtgard, and O. T. Saetre, in *Proceedings of the 38th IEEE Photovoltaic Specialists Conference* (IEEE, 2012), 505–508.

37. F. Mavromatakis, E. Kavoussanaki, F. Vignola, and Y. Franghiadakis, "Measuring and Estimating the Temperature of Photovoltaic Modules," *Solar Energy* 110 (2014): 656–666, https://doi.org/10.1016/j.solener.2014.10.009.

38. M. Jankovec and M. Topič, "Intercomparison of Temperature Sensors for Outdoor Monitoring of Photovoltaic Modules," *Journal of Solar Energy Engineering* 135 (2013): 031012, https://doi.org/10.1115/1.4023518.

39. I. M. Slauch, M. G. Deceglie, T. J. Silverman, and V. E. Ferry, in *Proceedings of the 46th IEEE Photovoltaic Specialists Conference (PVSC)* (IEEE, 2019).

40. N. Ammari, M. Mehdi, A. Alami Merrouni, and A. Benazzouz, "Experimental Analysis of Anti-Reflective Coating Performance in Desert Climate: Yield Analysis, Soiling Impact and Cleaning Durability Evaluation," *Sustainable Energy Technologies and Assessments* 60 (2023): 103547, https://doi.org/10.1016/j.seta.2023.103547.

18626319, 0, Downloaded from https://onlinelibrary.wiley.com/doi/10.1002/pssa.202500919 by Dtsch Zentrum F. Luft-U. Raum Fahrt In D. Helmholtz Gemein., Wiley Online Library on [27/11/2025]. See the Terms and Conditions (https://onlinelibrary.wiley.com/terms-and-conditions) on Wiley Online Library for rules of use; OA articles are governed by the applicable Creative Commons License

41. M. Fischer, M. Woodhouse, T. Brammer, P. Baliozian, International Technology Roadmap for Photovoltaics (ITRPV) (VDMA e. V., 2025).

42. G. Oreski, A. Omazic, G. C. Eder, et al., "Properties and Degradation Behaviour of Polyolefin Encapsulants for Photovoltaic Modules," *Progress in Photovoltaics* 28 (2020): 1277–1288, https://doi.org/10.1002/pip.3323.

43. G. Cattaneo, J. Levrat, H. Li, et al., in *Proceedings of the 47th IEEE Photovoltaic Specialists Conference (PVSC)* (IEEE, 2020), 1056–1061.

44. "*Datasheet L220, Pt-Temperatursensor nach DIN EN 60751*," Accessed September 9, 2025, https://www.yageogroup.com/content/datasheet/asset/file/YAGEO_Nexensos_L220_Datasheet_DE.

45. "*Grenzabweichungen der Genauigkeitsklassen F 0,6 / F 0,3 / F 0,15 / F 0,1. nach DIN EN IEC 60751*," Accessed September 9, 2025, https://www.yageo-nexensos.com/content/dam/nexensos/documents/technical_sensor_academy/technical_information/Tabelle_Abweichungen_DIN_EN_60751_100_Ohm_02-2001_DE.pdf.

46. "*Photovoltaic Geographical Information System*," Accessed November 19, 2025, https://re.jrc.ec.europa.eu/pvg_tools/en/.

47. "*Keysight 34970A/34972A Messdatenerfassungs-/Schaltsystem. Benutzerhandbuch*," Accessed September 9, 2025, https://www.keysight.com/us/en/assets/9018-02644/user-manuals/9018-02644.pdf.

48. "*Zero Volt Electronic Load. Application Note*," Accessed September 9, 2025, https://www.keysight.com/de/de/assets/7018-06815/application-notes/5968-6360.pdf.

Supporting Information

Additional supporting information can be found online in the Supporting Information section. **Supporting Table S1**. Process used for lamination of the modules. Temperature hot plate: 160 °C.

18626319, 0, Downloaded from https://onlinelibrary.wiley.com/doi/10.1002/pssa.202500919 by Dtsch Zentrum F. Luft-U. Raum Fahrt In D. Helmholtz Gemein., Wiley Online Library on [27/11/2025]. See the Terms and Conditions (https://onlinelibrary.wiley.com/terms-and-conditions) on Wiley Online Library for rules of use; OA articles are governed by the applicable Creative Commons License